

# Accepted Manuscript



MIR21 drives resistance to Heat Shock Protein 90 inhibition in cholangiocarcinoma

Andrea Lampis, Pietro Carotenuto, Georgios Vlachogiannis, Luciano Cascione, Somaieh Hedayat, Rosemary Burke, Paul Clarke, Else Bosma, Michele Simbolo, Aldo Scarpa, Sijia Yu, Rebecca Cole, Elizabeth Smyth, Javier Fernández Mateos, Ruwaida Begum, Blanka Hezelova, Zakaria Eltahir, Andrew Wotherspoon, Nicos Fotiadis, Maria Antonietta Bali, Chirag Nepal, Khurum Khan, Mark Stubbs, Jens C. Hahne, Pierluigi Gasparini, Vincenza Guzzardo, Carlo M. Croce, Suzanne Eccles, Matteo Fassan, David Cunningham, Jesper B. Andersen, Paul Workman, Nicola Valeri, Chiara Braconi

PII: S0016-5085(17)36331-X  
DOI: [10.1053/j.gastro.2017.10.043](https://doi.org/10.1053/j.gastro.2017.10.043)  
Reference: YGAST 61519

To appear in: *Gastroenterology*  
Accepted Date: 27 October 2017

Please cite this article as: Lampis A, Carotenuto P, Vlachogiannis G, Cascione L, Hedayat S, Burke R, Clarke P, Bosma E, Simbolo M, Scarpa A, Yu S, Cole R, Smyth E, Mateos JF, Begum R, Hezelova B, Eltahir Z, Wotherspoon A, Fotiadis N, Bali MA, Nepal C, Khan K, Stubbs M, Hahne JC, Gasparini P, Guzzardo V, Croce CM, Eccles S, Fassan M, Cunningham D, Andersen JB, Workman P, Valeri N, Braconi C, MIR21 drives resistance to Heat Shock Protein 90 inhibition in cholangiocarcinoma, *Gastroenterology* (2017), doi: 10.1053/j.gastro.2017.10.043.

This is a PDF file of an unedited manuscript that has been accepted for publication. As a service to our customers we are providing this early version of the manuscript. The manuscript will undergo copyediting, typesetting, and review of the resulting proof before it is published in its final form. Please note that during the production process errors may be discovered which could affect the content, and all legal disclaimers that apply to the journal pertain.

**MIR21 drives resistance to Heat Shock Protein 90 inhibition in cholangiocarcinoma.**

**Short title:** MIR21 as biomarker of resistance to HSP90 inhibition

Andrea Lampis<sup>1</sup>, Pietro Carotenuto<sup>1</sup>, Georgios Vlachogiannis<sup>1</sup>, Luciano Cascione<sup>2</sup>, Somaieh Hedayat<sup>1</sup>, Rosemary Burke<sup>1</sup>, Paul Clarke<sup>1</sup>, Else Bosma<sup>1</sup>, Michele Simbolo<sup>3</sup>, Aldo Scarpa<sup>3</sup>, Sijia Yu<sup>1</sup>, Rebecca Cole<sup>1</sup>, Elizabeth Smyth<sup>4</sup>, Javier Fernández Mateos<sup>1</sup>, Ruwaida Begum<sup>4</sup>, Blanka Hezelova<sup>4</sup>, Zakaria Eltahir<sup>4</sup>, Andrew Wotherspoon<sup>4</sup>, Nicos Fotiadis<sup>4</sup>, Maria Antonietta Bali<sup>4</sup>, Chirag Nepal<sup>5</sup>, Khurum, Khan<sup>4</sup>, Mark Stubbs<sup>1</sup>, Jens C Hahne<sup>1</sup>, Pierluigi Gasparini<sup>6</sup>, Vincenza Guzzardo<sup>7</sup>, Carlo M Croce<sup>6</sup>, Suzanne Eccles<sup>1</sup>, Matteo Fassan<sup>3,7</sup>, David Cunningham<sup>4</sup>, Jesper B Andersen<sup>5</sup>, Paul Workman<sup>1</sup>, Nicola Valeri<sup>1,4</sup>, Chiara Braconi<sup>1,4</sup>

<sup>1</sup> The Institute of Cancer Research, London, UK

<sup>2</sup> Bioinformatics Core Unit, Institute of Oncology Research, Bellinzona, Switzerland

<sup>3</sup> ARC-Net Research Centre and Department of Pathology and Diagnostics, University of Verona, Verona, IT

<sup>4</sup> The Royal Marsden NHS Trust London and Surrey, UK

<sup>5</sup> Biotech Research and Innovation Centre, Department of Health and Medical Sciences, University of Copenhagen, Copenhagen, DK

<sup>6</sup> Ohio State University, Columbus, USA

<sup>7</sup> Department of Medicine, University of Padua, Padua, IT

**Contact Information:** Chiara Braconi, Division of Cancer Therapeutics at The Institute of Cancer Research, London SM2 5NG. Phone: 0044 (0)2087224526. Fax: 0044 (0)2087224301 Email: [Chiara.braconi@icr.ac.uk](mailto:Chiara.braconi@icr.ac.uk).

**Conflict of interest:** PW and SE are members of the Project Team at ICR that developed AUY922 in collaboration with Vernalis.

**Transcriptomic profiling:** nanostring PDO (GEO accession number GSE102064 )

**Writing assistance:** we thank Nicky Evans for her editorial support

**Author contribution:** study concept and design (CB); acquisition of data (AL, PC, GV, SH, EB, MS, SY, RC, JFM, ZE, CN, JCH, PG, MF, VG); analysis and interpretation of data (LC,

CB, CN, JBA); drafting of the manuscript (AL); critical revision of the manuscript for important intellectual content (CB); statistical analysis (LC, CB); material support (RB, PC, AS, ES, RB, NF, MAB, KK, MS, CMC, SE, DC), obtained funding (CB, NV, DC, PW, AS).

**Grant Support:** Chiara Braconi is the recipient of an Institute of Cancer Research Clinician Scientist Fellowship, a Marie Curie Career Integration Grant from the European Union, an Early Diagnosis Award from Pancreatic Cancer Action and a NIHR Royal Marsden/ICR Biomedical Research Centre project grant. Nicola Valeri is a recipient of a CRUK Career Development Award, a NIHR Royal Marsden/ICR Biomedical Research Centre Flagship Grant, and a Marie Curie Career Integration Grant from the European Union. Aldo Scarpa is a recipient of an Associazione Italiana Ricerca sul Cancro (AIRC) grant n. 12182. JBA holds a Novo Nordisk Foundation Hallas-Møller fellowship. CN holds a postdoctoral fellowship from the Danish Medical Research Council (DFF). We acknowledge Cancer Research UK funding to the Cancer Research UK Cancer Therapeutics Unit at the Institute of Cancer Research. Paul Workman is a Cancer Research UK Life Fellow.

#### List of Abbreviations

*ARID1*, AT-rich interactive domain  
*BAP1*, BRCA1 associated protein 1  
 CCA, cholangiocarcinoma  
 CRC, colorectal cancer  
 CTRL, control  
 dCCA, distal cholangiocarcinoma  
*DNAJB5*, DnaJ homolog subfamily B member 5  
 eCCA, extrahepatic cholangiocarcinoma  
 EGF, Epidermal Growth Factor  
 FFPE, Formalin Fixed Paraffin Embedded  
 GEM, gemcitabine  
 GI, Growth Inhibition  
*FGFR*, fibroblast growth factor receptor  
 HDAC, histone deacetylases  
 H&E, Hematoxylin and eosin  
 HGF, Hepatocytes Growth Factor  
 HSP, heat shock protein  
 HTS, high-throughput screening  
 iCCA, intrahepatic cholangiocarcinoma  
*IDH1*, isocitrate dehydrogenase 1 (NADP+)  
 MIR21, microRNA 21  
 MIR21KO, a homozygous *MIR21* knockout

MUT, mutant

*PBRM1*, polybromol

pCCA, perihilar cholangiocarcinoma

PDO, patients derived organoids

*PI3K*, phosphatidylinositol-4,5-bisphosphate 3-kinase

SD, standard deviation

*TP53*, tumor protein p53

WT, wild type

ACCEPTED MANUSCRIPT

**Abstract**

**Background & Aims:** Cholangiocarcinomas (CCA) are resistant to chemotherapy, so new therapeutic agents are needed. We performed a screen to identify small molecule compounds that are active against CCAs. Levels of microRNA 21 (MIR21 or miRNA21) are increased in CCAs. We investigated whether miRNA21 mediates resistance of CCA cells and organoids to HSP90 inhibitors.

**Methods:** We performed a high-throughput screen of 484 small molecule compounds to identify those that reduced viability of 6 human CCA cell lines. We tested the effects of HSP90 inhibitors on cells with disruption of the *MIR21* gene, cells incubated with MIR21 inhibitors, and stable cell lines with inducible expression of MIR21. We obtained CCA biopsies from patients, cultured them as organoids (patient-derived organoids, PDOs). We assessed their architecture, mutation and gene expression patterns, response to compounds in culture, and when grown as subcutaneous xenograft tumors in mice.

**Results:** Cells with *IDH1* and *PBRM1* mutations had the highest level of sensitivity to histone deacetylase inhibitors. HSP90 inhibitors were effective in all cell lines, irrespective of mutations. Sensitivity of cells to HSP90 inhibitors correlated inversely with baseline level of MIR21. Disruption of MIR21 increased cell sensitivity to HSP90 inhibitors. CCA cells that expressed transgenic MIR21 were more resistant to HSP90 inhibitors than cells transfected with control vectors; inactivation of MIR21 in these cells restored sensitivity to these agents. MIR21 was shown to target the DnaJ heatshockprotein family (Hsp40) member B5 (DNAJB5). Transgenic expression of DNAJB5 in CCA cells that overexpressed MIR21 re-sensitized them to HSP90 inhibitors. Sensitivity of PDOs to HSP90 inhibitors, in culture and when grown as xenograft tumors in mice, depended on expression of miRNA21.

**Conclusions:** miRNA21 appears to mediate resistance of CCA cells to HSP90 inhibitors by reducing levels of DNAJB5. HSP90 inhibitors might be developed for treatment of CCA and miRNA21 might be a marker of sensitivity to these agents.

**KEY WORDS:** organoid, AUY922, bile duct cancer, DNAJB5

Cholangiocarcinomas (CCA) are tumours with dismal prognosis<sup>1-4</sup>. Surgery is the only curative treatment modality in CCA; however, less than 30 % of patients are diagnosed with resectable disease<sup>5, 6</sup>. In advanced CCA the efficacy of systemic treatment is limited by drug-resistance<sup>5</sup>. A combination treatment with cisplatin and gemcitabine is recommended as first-line standard for patients with inoperable CCAs, based on data from the ABC-02 trial<sup>7-9</sup>. However, long term outcome is still poor<sup>5</sup>, highlighting the need for the identification of novel therapeutics along with appropriate strategies for clinical implementation.

Attempts to test the efficacy of targeted therapies and small molecules against CCAs have been made without a proper phase of target selection and validation, leading to repeated failures in small and unselected populations of CCA patients<sup>10-13</sup>. Notably, a phase III trial failed to show a benefit from the addition of erlotinib to a gemcitabine-platinum combination in metastatic CCAs that were not enriched for the appropriate molecular subtype<sup>14</sup>.

Molecularly targeted small molecule drugs are low molecular-weight compounds that regulate biological processes and can rapidly diffuse across cell membranes so that they can reach intracellular sites of action<sup>15</sup>. Small molecules have entered clinical practice for the treatment of other forms of solid malignancies, where the dependence of the cancer on specific pathways is understood. Here, we report data from a high-throughput screen (HTS) of a library of small molecule drugs and chemical tools in human CCA cell lines that have been genetically characterized for the most frequent mutations observed in human CCA, along with validation in *ex vivo* and *in vivo* models of promising compounds and relative biomarkers of response. Our approach has enabled us to identify molecularly targeted small molecules that have activity against CCAs and related biomarkers that may inform future clinical trial design.

## Experimental Procedures

**High-throughput-screening (HTS).** A custom compound library including 484 small molecules was developed in the Cancer Research UK Cancer Therapeutics Unit at the Institute of Cancer Research (Supporting Table S1). Cells were plated into a polypropylene 384-well assay plate (Greiner Bio-One, Frickenhausen, Germany) for 48 hours before compounds were screened at the final concentration of 80nM, 200nM and 800nM in 0.3% (v/v) DMSO by dispensing 125 nL compound solution from a source plate containing the compounds at a concentration of 32 $\mu$ M, 80 $\mu$ M and 320 $\mu$ M in 2% (v/v) DMSO, into the central 320 wells of a 384-plate. 0.3% (v/v) DMSO was used as a vehicle control. Cell viability was assessed 72 hours later by fluorimetric assay (CellTiter-Blue, Promega Madison, WI, USA). The cell viability measurement from each hit was normalized to those of cells exposed to vehicle only. Each cell line was tested in triplicate. Statistical significance ( $p < 0.05$ ) was determined by two-sided t-test across 3 replicates.

**Statistical analyses.** Statistical analyses were performed by GraphPad Prism 6 (La Jolla, CA, USA). Results are expressed as mean  $\pm$  SD, unless indicated otherwise. Groups that were normally distributed were compared with either a 2-tailed Student's *t* test (for analysis of 2 groups) or using 2-way ANOVA to compare multiple groups. Non-parametric data were analyzed using a Wilcoxon–Mann-Whitney *U* test when comparing 2 groups. Significance was accepted when *p* was less than 0.05.

**Patient-derived organoids (PDO).** One core biopsy was obtained from a patient with advanced iCCA after ethical approval within the CCR3689 protocol at the Royal Marsden Hospital. For the colorectal cancer (CRC) PDOs one core biopsy was obtained from a liver metastasis of a chemo-refractory colorectal cancer patient (protocol CCR4164). The biopsy was minced, conditioned in PBS/EDTA 5 mM for 15 min at room temperature, and digested in PBS/EDTA containing 2x TrypLe (Thermo Fisher Scientific, Waltham, MA, USA) for 1

hr at 37 °C. Following digestion, mechanical force was applied in order to facilitate cell release in solution. Dissociated cells were collected in Advanced DMEM/F12 (Thermo Fisher Scientific, Waltham, MA, USA), suspended in growth factor reduced (GFR) matrigel (Corning Inc., Corning, NY, USA), and seeded. The matrigel was then solidified and overlaid with 500 µl of complete human organoid medium, which was subsequently refreshed every two days. PDOs were cultured in Advanced DMEM/F12, supplemented with 1x B27 additive and 1x N2 additive (Thermo Fisher Scientific, Waltham, MA, USA), 0.01% bovine serum albumine, 2 mM L-glutamine, 100 units/ml penicillin-streptomycin, and containing the following additives: EGF, noggin, R-spondin 1, gastrin, FGF-10, FGFF-basic, Wnt-3A, prostaglandin E2, Y-27632, nicotinamide, A83-01, A83-01, SB202190, HGF (Pepro-Tech, London, UK). Passaging of PDOs was performed using TrypLe. PDOs were biobanked in FBS (Thermo Fisher Scientific, Waltham, MA, USA), containing 10% DMSO (Sigma-Aldrich, St Louis, MI, USA).

***PDO histology.*** PDOs were harvested out of matrigel by inoculating them with 1 ml of Cell Recovery Solution (Corning Inc., Corning, NY, USA) for 60 min at 4 °C. Organoids were then collected in cold PBS, pelleted, and fixed in Formalin 10% (Sigma-Aldrich, St Louis, MI, USA) for 60 min. Following fixation, organoids were washed and resuspended in 200 µl of warm agarose 2%. The agarose pellet was dehydrated using ethanol, and embedded in paraffin using a standard histological protocol.

***PDO NanoString analysis.*** 100 ng of total RNA extracted from PDOs and matching FFPE biopsies were run with the nCounter PanCancer Progression panel (Nanostring Technologies, Seattle, WA, USA), according to the manufacturer's instructions. Raw data were normalised using the NanoStringNorm R package version 1.1.21 following recommended parameters and median centred by genes.

**PDO targeting sequencing.** DNA and RNA were extracted using the Qiagen AllPrep DNA/RNA/miRNA Universal kit (Qiagen, Hilden, Germany). Targeted library preparation and DNA-sequencing were outsourced to GATC Biotech. In brief, DNA libraries were prepared with the ClearSeq Comprehensive Cancer panel (Agilent Technologies, Santa Clara, CA, USA) that targets 151 cancer-related genes, using SureSelectV6 chemistry (Agilent Technologies, Santa Clara, CA, USA). Paired-end sequencing (2 x 125 bp) was then performed using Illumina technology.

**3D organoid compound assay and screening.** Organoids (30 µl of GFR matrigel containing 6,000 cells) were seeded in 96-well cell culture plates; after matrigel solidified it was overlaid with 70 µl of complete human organoid medium. Complete medium was refreshed once after 24 h. Compound was added 3 days later and compound-containing medium was further refreshed every 2 days. After 11 days medium was removed and replaced with 100 µl of complete human organoid medium containing 10% CellTiter-Blue Cell Viability Assay (Promega, Madison, WI, USA). The organoid compound screen was conducted in 96-well cell culture plates using a custom-made library of 55 compounds and 5 DMSO controls; it was conducted in triplicate, using a concentration of 1 µM for all compounds.

**PDO-derived xenografts.** All *in vivo* experiments were performed in accordance with the local ethical review panel, the UK Home Office Animals (Scientific Procedures) Act 1986, the United Kingdom National Cancer Research Institute guidelines for the welfare of animals in cancer research<sup>13</sup>, and the ARRIVE guidelines. Further details about animal experiments and additional methods can be found in the supporting information. Animals were housed in specific pathogen-free rooms in autoclaved, aseptic microisolator cages with a maximum of five animals per cage. Food and water were provided *ad libitum*. 100 µl of matrigel containing ~20,000 small MIR21 TRIPZ organoids were injected subcutaneously in the flank of 6-7 weeks old NOD *scid* gamma (NSG) animals (Charles River Laboratories, Wilmington,

MA, USA) while they were kept on doxycycline diet [LabDiet 5053 w/ 1250 ppm doxycycline blue (LabDiet, St Louis, MO, USA)]. About 10 weeks post inoculation tumours were passaged and equal fragments of tumours were implanted subcutaneously into a next generation of mice to obtain a total of 18 mice. Eight mice were treated with vehicle, while 10 mice were treated with AUY922 (25mg/kg intraperitoneally) three times a week. After two weeks, mice were randomized to stay on doxycycline diet or to move onto a doxycycline-free diet for other two weeks while treatment was continued. Tumour volume was determined using the following formula:  $=4.19 \times (\text{diam1} / 4 + \text{diam2} / 4)^3$ . After 4 weeks of treatment mice were culled and their tumours were excised, fixed in formalin, and embedded in paraffin.

## **Results**

### ***HTS with a small molecule compound library identified vulnerabilities that can be exploited for novel therapeutics in CCA.***

To explore the activity of small molecules in CCA we screened a library of 484 molecularly targeted small molecule compounds (Supporting Table S1) for their effect on the viability of human CCA cell lines. Both intrahepatic (iCCA) and extrahepatic (eCCA) CCA cell lines were included. Next-generation-sequencing revealed that these cell lines were representative of human CCA tissues. We used a 64-gene panel that included the most frequently mutated genes in human CCA<sup>16</sup>, and found that mutations that are present in >10% in human tissues were represented in our cell lines, with the exceptions of *ARID1* (Figure 1A & Supporting Table S2). EGI-1, TFK-1, SNU-1196, SW1, CCLP, and SNU-1079 were selected for the screening in view of their origin, and their growth rate and pattern.

Compounds were screened at three different concentrations (80 nM, 200 nM, 800 nM) in triplicate for each cell line. A number of compounds (median = 68 per cell line) had a significant effect on cell viability at all concentrations tested (Supporting Table S3 & Figure 1B). Gemcitabine, a well-known active drug in CCA, had significant activity at all concentrations tested, in each cell line, confirming the validity of our approach (Figure 1C). In order to assess which pathway may be more relevant as a potential target of therapy in CCA, we grouped compounds with different chemical structure that acted on the same molecular target and investigated if there was an enrichment in selected molecular pathways amongst the drugs that were significantly active across the cell lines<sup>17, 18</sup> (Figure 1D). We observed enrichment for microtubule associated compounds and mTOR inhibitors in all cell lines. Clinical trials are ongoing for microtubule-targeted compounds such as Nab-Paclitaxel and mTOR inhibitors such as Everolimus. Interestingly, there was an enrichment of histone-deacetylase (HDAC) inhibitors among the hits in the SNU-1079 cell line, which harbors mutations in the isocitrate dehydrogenase 1 (*IDH1*) and polybromo1 (*PBRM1*) chromatin remodeling genes. In line with previous data<sup>19</sup>, SNU-1079 cells also showed hypersensitivity to dasatinib (Supporting Table S3). A number of EGFR inhibitors had a significant effect on the viability of SW1, SNU-1196 and TFK cell lines. Interestingly both aurora kinase and heat shock protein (HSP)90 inhibitors were effective in all cell lines.

***Association between mutational status of CCA cell lines and their sensitivity to selected compounds.***

In order to investigate whether selected mutations were associated with sensitivity to specific targeted agents, we ran an analysis for *BRCA* Associated Protein (*BAP1*) and *TP53* mutations as these were present in more than one cell line (Supporting Figure S1A&B). Our analysis revealed that *BAP1*-mutant (MUT) CCA cell lines were more sensitive ( $p < 0.05$ ) to a range of

small-molecules that include compounds with activity of PI3K pathway: SANT-2 (SMO antagonist), ABT-737 (inhibitor of Bcl-(X)L, Bcl-2 and Bcl-W), LY294002 (PI3K $\alpha/\beta/\delta$  inhibitor), PIK-93 (PI3K $\alpha/\gamma$  inhibitor), SB203580 (p38 MAPK inhibitor) and SB590885 (BRAF inhibitor). *TP53*-MUT cells did not show any increased sensitivity to the compounds we screened in comparison to WT cells. However, we noticed a significant ( $p < 0.05$ ) correlation between mutations in *TP53* and resistance to PF-573228 (ATP-competitive inhibitor of FAK), ABT-263 (Navitoclax, a potent inhibitor of Bcl-(X)L, Bcl-2 and Bcl-W) and MM-102 (MLLT1 inhibitor). The limited number of cell lines does not enable to draw definitive conclusions, even though these findings suggest potential associations that may deserve further investigation.

#### ***FGFR-targeting compounds in CCA cell lines.***

Given emerging data on the activation of the fibroblast growth factor receptor (FGFR) pathway in CCA<sup>20-23</sup>, we looked at the effect on cell viability of the six compounds in our screen that act on FGFR. The effect of these compounds on cell viability was most consistent at the highest concentration tested, 800 nM (Figure 2A). Whilst brivanib (VEGFR/FGFR inhibitor) and the multi-kinase inhibitor pazopanib had no effect, both danusertib (a pan-aurora kinase inhibitor with an off-target effect on FGFR1) and ponatinib (a Src and Bcr-Abl kinase inhibitor with activity on all 4 FGFRs)<sup>24</sup> reduced CCA cell viability. However, we acknowledge that our system may not be ideal for the assessment of angiogenesis/stroma-directed drugs and that our cells are not known to carry FGFR2 alterations.

#### ***HSP90 inhibitors are effective in CCA cell lines.***

We have previously observed enrichment in AK and HSP90 inhibitors amongst the significant hits of our CCA HTS. While AK inhibitors appear to be quite toxic in solid

tumours<sup>25</sup>, a recent report showed that HSP90 inhibition is effective and tolerable in *in vivo* CCA preclinical models<sup>26</sup>. HSP90 inhibition is attractive in CCA as HSP90 interacts with and controls a variety of client proteins that play key role in CCA pathogenesis such as EGFR, PTEN, PI3K, HER2, HER3, and PRKA. Moreover, recent evidence suggests that HSP90 inhibition is remarkably effective in tumours with FGFR fusions and activation of the IL6/STAT pathway<sup>27, 28</sup>.

Our small molecule compound library included nine HSP90 inhibitors including those from different chemical series, and 78% were active across our CCA cell line panel, with the highest activity recorded for AUY922, 17-AAG, 17-DMAG, ganetespib and BIIB021 (Figure 2A). Notably, the Growth Inhibitory GI<sub>50</sub> of AUY922, a potent HSP90 inhibitor<sup>29</sup>, was in the nanomolar range in all of the CCA cell lines tested (Figure 2B). We could not find any correlation between the most frequent mutations in CCA and the activity of the HSP90 inhibitors in our CCA cell lines.

***MIR21 as driver of resistance to HSP90 inhibitors.*** Previously, microRNAs (miRNA) have been shown to modulate drug sensitivity and to act as biomarkers of drug response<sup>1, 4, 30-37</sup>. MIR21 is an oncogenic miRNA that drives cholangiocarcinoma pathogenesis and sensitization to conventional chemotherapy drugs<sup>38, 39</sup>. Thus, we investigated if MIR21 could be used as a biomarker of response to HSP90 inhibition in CCA. Interestingly, we noticed that MIR21 expression reflected the sensitivity of CCA cells to AUY922, as cell lines with high levels of MIR21 expression had higher GI<sub>50</sub> values for AUY922 (Figure 2C). Sensitivity to AUY922 was significantly increased in CCA cells transfected with a locked nucleic acid (LNA) MIR21 inhibitor compared with those transfected with a negative control LNA (Figure 2D). To validate the relationship between MIR21 expression and AUY922 sensitivity we ran a high-throughput compound screen in RKO cells which had been engineered to

knock out the *MIR21* locus (MIR21KO), and parental isogenic wild type (WT) cells<sup>40</sup>. A number of HSP90 inhibitors produced a larger reduction in cell viability in MIR21KO cells in comparison to WT cells (Supporting Figure S2A), with AUY922, 17-AAG, 17-DMAG, and ganetespib showing the highest activity. When treated with HSP90 inhibitors, MIR21KO RKO cells were more sensitive than WT RKO cells (Supporting Figure S2B). Correspondingly, the GI<sub>50</sub> for AUY922 was found to be 35 nM in WT cells and 17 nM in MIR21KO cells (Supporting Figure S2C). Interestingly, we could detect no difference in the sensitivity to AUY922 in WT and MIR21KO DLD1 cells, which is consistent with the lower baseline level of MIR21 in DLD-1 cells and their likely lower dependence on MIR21 (Supporting Figure S2D). Indeed, DLD-1 WT cells were more sensitive to AUY922 than RKO WT, while silencing of MIR21 in RKO cells restored their sensitivity (Supporting Figure S2E&F).

In order to validate the role of MIR21 in driving resistance to HSP90 inhibition, we infected MIR21KO DLD-1 cells with an inducible MIR21 or control (CTRL) viral vector (Supporting Figure S2F) and monitored their response to AUY922. Enforced expression of MIR21 significantly increased resistance to AUY922 ( $p < 0.05$ ), when compared to the effect of infection with an empty CTRL vector (Supporting Figure S3A and Supporting Video 1). Indeed, in co-culture with non-infected MIR21KO DLD-1 cells, MIR21 induced DLD-1 cells could proliferate in the presence of AUY922 (Supporting Figure S3B and Supporting Video 2). To ascertain if these results could be extended to CCA, we generated Tet-on inducible clones for the over-expression of MIR21 in the CCLP cell line (Figure 2E). In line with previous data, CCLP cells with enforced expression of MIR21 were significantly more resistant to AUY922 than cells transfected with the CTRL vector. Accordingly, deactivation of the Tet-on system restored sensitivity to AUY922 in CCLP cells (Figure 2F&G,

Supporting Table S4). Comparable data were also obtained in the EGI CCA cell line (Supporting Figure S4).

***DNAJB5 is a mediator of MIR21 dependent resistance to AUY922.***

To gain insight into the relationship between MIR21 and the HSPs, we measured the expression levels of a panel of HSPs and co-chaperones in Tet-on MIR21 vector CCLP cells treated with AUY922. A multiplex sandwich immunoassay showed a reduction in the level of HSP40 (encoded by DnaJ heat shock protein family (Hsp40) member B5, *DNAJB5*) in MIR21 vector cells compared with CTRL cells (Figure 3A). *In silico* analysis of the *DNAJB5* sequence revealed a binding site for MIR21 within its 3'UTR (Figure 3B). Western blot analysis confirmed induction of *DNAJB5* upon AUY922 treatment and reduction in *DNAJB5* expression in MIR21 over-expressing cells (Figure 3C), and a luciferase reporter assay confirmed a direct interaction between MIR21 and the 3'UTR of *DNAJB5* (Figure 3D). Interestingly, enforced expression of *DNAJB5* in MIR21 over-expressing cells re-sensitized CCLP cells to AUY922 (Figure 3E), confirming that *DNAJB5* may be a mediator of MIR21-induced resistance.

***Correlation between MIR21 expression and sensitivity to AUY922 in patient-derived organoids (PDOs) and PDO-derived xenografts.***

Patient-derived organoids (PDOs) have recently emerged as organotypic cultures that recapitulate the complex three-dimensional organization of cancer better than 2D tumour cell lines<sup>41-43</sup>. To assess the clinical relevance of our findings, we tested AUY922 activity in PDOs established from the liver biopsy of a chemoresistant iCCA patient (Figure 4 & Figure 5A). PDOs retained the same morphology of the primary tumour (Figure 5B), as well the same positivity for cytokeratin 7 and 19 (Figure 5C and Figure 4B). Gene expression

profiling showed that the transcriptome of PDOs recapitulated that of the primary tissue [with a Spearman  $r$  score of 0.91 for the housekeeping genes, and 0.61 for the whole transcriptome ( $p < 0.0001$ )] (Figure 5D). DNA sequencing confirmed that the genetic background of the PDOs matched that of the primary biopsy, with a Spearman  $r$  score of 0.96 for SNVs (Figure 5E). CCA PDOs were tested against a panel of small molecule compounds and confirmed resistance to fluorouracil and oxaliplatin that patient had received before the development of PDO (Figure 5F). CCA PDOs were sensitive to AUY922 (Figure 5F&G), and this sensitivity was significantly enhanced after inducible inhibition of MIR21 (Figure 5H&I). In parallel PDOs derived from a colorectal cancer patient with low endogenous expression of MIR21 were characterised (personal data) and tested against AUY922 before and after MIR21 expression confirming the relationship between miRNA expression and sensitivity to HSP90 inhibition (Supporting Figure S5). Next, we generated CCA PDO-derived tumour xenografts by inoculating Tet-on MIR21 PDOs in the flank of NSG mice. Mice were treated with AUY922 or vehicle while changes in their diet were applied to modulate the expression of MIR21. After two weeks of treatment mice were randomized to stay on doxycycline diet (DOX-ON) or changed to a doxycycline -free (DOX-OFF) diet. While a non-significant change was observed for vehicle-treated mice, AUY922-treated mice on DOX-OFF diet achieved a significantly better tumour response than animals which remained on a doxycycline diet (Figure 6A&B&C & Supporting Table S5). MIR21 expression was confirmed to be inactivated in the tumour after withdrawal of doxycycline diet, while an increase in DNAJB5 protein expression was detected (Figure 6D).

## Discussion

The best way to treat advanced CCA is still a matter of debate within the clinical and scientific community<sup>5, 6</sup>. The ABC-02 trial has proved the efficacy of platinum-gemcitabine combination chemotherapy in the first line setting<sup>7</sup>. However, a series of clinical trials have failed to demonstrate any benefit from targeted therapies in CCA<sup>11, 12, 14, 44</sup>. Despite advances having been made in the genetic and molecular characterization of biliary tract cancers, none of the clinical trials were designed with an appropriate strategy of patients' selection based on pre-clinical evidence. In this study, we explored the activity of a plethora of small molecule compounds and probes that have shown activity in other cancers. In this way, we hoped to identify drug candidates and appropriate biomarkers for use in, and to aid patient selection for, future clinical trials. We propose that the decision to use targeted therapies should be based on the molecular characterization of a tumour, rather than its site of origin. Hence, in this study we included cell lines originating from all types of cholangiocarcinoma.

As expected we did observe significant activity for gemcitabine and compounds which impair microtubule dynamics and cause cell cycle arrest. We also found that compounds which inhibit mTOR signalling had activity in CCA cell lines, consistent with previous evidence suggesting that the mTOR pathway is involved in cholangiocarcinoma tumorigenesis and that sirolimus may induce partial remissions in CCA patients<sup>45, 46</sup>. Nonetheless, we did not focus on these compounds given that clinical trials are ongoing and may provide additional insights. The observation that HDAC inhibitors were enriched amongst the hits in SNU-1079 cells was in line with previous observations on the effect of *IDH* mutations on the impairment of histone demethylation<sup>47</sup>.

We and colleagues at The Institute of Cancer Research have an interest in the therapeutic applications of HSP90 inhibitors and biomarkers of sensitivity to these agents, and we co-discovered the highly potent and selective HSP90 inhibitor AU922<sup>48</sup>. Shirota et al. have

recently shown that HSP90 inhibitors have potent *in vitro* and *in vivo* anti-proliferative activity in CCA<sup>26</sup>, prompting us to investigate potential biomarkers of sensitivity to HSP90 inhibition in our study. HSP90 inhibitors, including AUY922, have shown an acceptable toxicity profile in humans in phase I clinical trials<sup>49-51</sup>, and are currently investigated in phase II clinical trials for lung and breast cancers. To date, no reports are available on the role of AUY922 in biliary tract cancer patients. More interestingly, growing evidence points to a role of HSP90 inhibitors in facilitating the anti-tumour activity of immune cells<sup>52, 53</sup>. We showed that CCAs are characterized by an immuno-deregulation that creates an immunosuppressive milieu<sup>54</sup>; thus HSP90 may be used to reactivate an anti-tumour response in CCA. HSP90 is a key component in a multi-chaperone complex involved in the post-translational folding of a number of client proteins, including microRNA-regulated proteins such as argonaute2 (AGO2)<sup>55-57</sup>. We reasoned microRNAs may be good biomarker candidates given their capacity to act on several HSP90-associated proteins that drive tumorigenesis and drug resistance. MIR21 was previously shown to modulate cytotoxic drug response<sup>58</sup> and is predicted to target genes that act as client proteins for HSP90<sup>2, 3, 20, 21, 38, 59</sup>. However, microRNAs have never been studied as mediators of the response to HSP90 inhibitors<sup>60</sup>. We observed that MIR21 can drive tumour cell proliferation in the presence of HSP90 inhibitors. Our data suggest that it would be useful to carry out further studies of the biomarker potential of MIR21 as a guide treatment with HSP90 inhibitors, as well as to pursue the combination of HSP90 inhibitors with MIR21 inhibitors in CCA. Moreover, our data suggest a generalized mechanism of resistance to HSP90 inhibition and may be applied to second generation HSP90 inhibitors that may be clinically more attractive<sup>61, 62</sup>. HSP70 is a well-known compensatory mechanism of HSP90 inhibition. The stress-inducible HSP70 is central in promoting protein folding. As elegantly described by Hartl *et al*<sup>63</sup> HSP70 is responsible for the initial folding of substrates and their loading into HSP90. Its affinity for unfolded

substrates is tightly regulated by HSP40. Indeed, not only HSP40 delivers unfolded substrates to ATP-bound HSP70, but it also accelerates the hydrolysis of ATP inducing a tighter binding of the substrate by HSP70. We speculate that MIR21 can interfere with this balance and thus, with the HSP90-mediated activation of client proteins, by modulating the expression of HSP40.

We have shown here that MIR21 drives resistance both in CCA and in non-CCA carcinoma cells. Thus, it is likely that these findings may be extended to a number of malignancies. Despite a general over-expression of MIR21 in cancer tissues, it is known that MIR21 is remarkably over-expressed in a proportion of cancer patients and may therefore serve as a valuable biomarker<sup>39</sup>. In addition, there is evidence that levels of circulating MIR21 can define the prognosis of cancer patients and may act as surrogate for miRNA expression in the tumour<sup>34</sup>. Thus, circulating MIR21 may represent an easily accessible tool for the identification of patients likely to benefit from treatment with HSP90 inhibitors.

Finally, we have provided initial evidence of the feasibility of developing human PDOs from cholangiocarcinoma patients. To date, successful 3D organoids have been established from a variety of cancer types, but no evidence has been reported for biliary tract cancers. In these studies we show that PDOs could be derived from one biopsy core indicating that this technology may be attractive for clinical implementation. Our studies indicate the possibility that PDOs may resemble the original tumour and may potentially be used for *in vitro* application and manipulation within 6-8 weeks from establishment. Thus, it may represent a promising novel tool to guide treatment selection within the life expectancy of cholangiocarcinoma patients and offer an additional platform that better recapitulates human cancers to investigate their biology.

## Acknowledgments

We acknowledge the contribution of our ICR colleagues Swee Sharp, Marissa Powers, and Rob van Montfort for making available reagents and for access to equipment. We thank Bernadett Kolozsvari from Essen Bioscience for her support with the Incucyte analysis and Nicky Evans for editorial assistance.

## References

1. Banales JM, Cardinale V, Carpino G, et al. Expert consensus document: Cholangiocarcinoma: current knowledge and future perspectives consensus statement from the European Network for the Study of Cholangiocarcinoma (ENS-CCA). *Nat Rev Gastroenterol Hepatol* 2016;13:261-80.
2. Braconi C, Patel T. Cholangiocarcinoma: new insights into disease pathogenesis and biology. *Infect Dis Clin North Am* 2010;24:871-84, vii.
3. Braconi C, Swenson E, Kogure T, et al. Targeting the IL-6 dependent phenotype can identify novel therapies for cholangiocarcinoma. *PLoS One* 2010;5:e15195.
4. Braconi C, Huang N, Patel T. MicroRNA-dependent regulation of DNA methyltransferase-1 and tumor suppressor gene expression by interleukin-6 in human malignant cholangiocytes. *Hepatology* 2010;51:881-90.
5. Bridgewater J, Galle PR, Khan SA, et al. Guidelines for the diagnosis and management of intrahepatic cholangiocarcinoma. *J Hepatol* 2014;60:1268-89.
6. Razumilava N, Gores GJ. Cholangiocarcinoma. *Lancet* 2014;383:2168-79.
7. Valle J, Wasan H, Palmer DH, et al. Cisplatin plus gemcitabine versus gemcitabine for biliary tract cancer. *N Engl J Med* 2010;362:1273-81.

8. Valle JW, Furuse J, Jitlal M, et al. Cisplatin and gemcitabine for advanced biliary tract cancer: a meta-analysis of two randomised trials. *Ann Oncol* 2014;25:391-8.
9. Okusaka T, Nakachi K, Fukutomi A, et al. Gemcitabine alone or in combination with cisplatin in patients with biliary tract cancer: a comparative multicentre study in Japan. *Br J Cancer* 2010;103:469-74.
10. El-Khoueiry AB, Rankin C, Siegel AB, et al. S0941: a phase 2 SWOG study of sorafenib and erlotinib in patients with advanced gallbladder carcinoma or cholangiocarcinoma. *Br J Cancer* 2014;110:882-7.
11. Malka D, Cervera P, Foulon S, et al. Gemcitabine and oxaliplatin with or without cetuximab in advanced biliary-tract cancer (BINGO): a randomised, open-label, non-comparative phase 2 trial. *Lancet Oncol* 2014;15:819-28.
12. Valle JW, Wasan H, Lopes A, et al. Cediranib or placebo in combination with cisplatin and gemcitabine chemotherapy for patients with advanced biliary tract cancer (ABC-03): a randomised phase 2 trial. *Lancet Oncol* 2015;16:967-78.
13. Bridgewater J, Lopes A, Beare S, et al. A phase 1b study of Selumetinib in combination with Cisplatin and Gemcitabine in advanced or metastatic biliary tract cancer: the ABC-04 study. *BMC Cancer* 2016;16:153.
14. Lee J, Park SH, Chang HM, et al. Gemcitabine and oxaliplatin with or without erlotinib in advanced biliary-tract cancer: a multicentre, open-label, randomised, phase 3 study. *Lancet Oncol* 2012;13:181-8.
15. Hoelder S, Clarke PA, Workman P. Discovery of small molecule cancer drugs: successes, challenges and opportunities. *Mol Oncol* 2012;6:155-76.
16. **Simbolo M, Fassan M, Ruzzenente A, et al. Multigene mutational profiling of cholangiocarcinomas identifies actionable molecular subgroups. *Oncotarget* 2014;5:2839-52.**

17. Workman P, Collins I. Probing the probes: fitness factors for small molecule tools. *Chem Biol* 2010;17:561-77.
18. Blagg J, Workman P. Choose and Use Your Chemical Probe Wisely to Explore Cancer Biology. *Cancer Cell* 2017;32:268-270.
19. Saha SK, Gordan JD, Kleinstiver BP, et al. Isocitrate Dehydrogenase Mutations Confer Dasatinib Hypersensitivity and SRC Dependence in Intrahepatic Cholangiocarcinoma. *Cancer Discov* 2016;6:727-39.
20. Sia D, Losic B, Moeini A, et al. Massive parallel sequencing uncovers actionable FGFR2-PPHLN1 fusion and ARAF mutations in intrahepatic cholangiocarcinoma. *Nat Commun* 2015;6:6087.
21. Goyal L, Saha SK, Liu LY, et al. Polyclonal Secondary FGFR2 Mutations Drive Acquired Resistance to FGFR Inhibition in Patients with FGFR2 Fusion-Positive Cholangiocarcinoma. *Cancer Discov* 2017;7:252-263.
22. Borad MJ, Champion MD, Egan JB, et al. Integrated genomic characterization reveals novel, therapeutically relevant drug targets in FGFR and EGFR pathways in sporadic intrahepatic cholangiocarcinoma. *PLoS Genet* 2014;10:e1004135.
23. Wang Y, Ding X, Wang S, et al. Antitumor effect of FGFR inhibitors on a novel cholangiocarcinoma patient derived xenograft mouse model endogenously expressing an FGFR2-CCDC6 fusion protein. *Cancer Lett* 2016;380:163-73.
24. Gozgit JM, Wong MJ, Moran L, et al. Ponatinib (AP24534), a multitargeted pan-FGFR inhibitor with activity in multiple FGFR-amplified or mutated cancer models. *Mol Cancer Ther* 2012;11:690-9.
25. Bavetsias V, Linardopoulos S. Aurora Kinase Inhibitors: Current Status and Outlook. *Front Oncol* 2015;5:278.

26. Shirota T, Ojima H, Hiraoka N, et al. Heat Shock Protein 90 Is a Potential Therapeutic Target in Cholangiocarcinoma. *Mol Cancer Ther* 2015;14:1985-93.
27. Lin H, Kolosenko I, Bjorklund AC, et al. An activated JAK/STAT3 pathway and CD45 expression are associated with sensitivity to Hsp90 inhibitors in multiple myeloma. *Exp Cell Res* 2013;319:600-11.
28. Acquaviva J, He S, Zhang C, et al. FGFR3 translocations in bladder cancer: differential sensitivity to HSP90 inhibition based on drug metabolism. *Mol Cancer Res* 2014;12:1042-54.
29. Eccles SA, Massey A, Raynaud FI, et al. NVP-AUY922: a novel heat shock protein 90 inhibitor active against xenograft tumor growth, angiogenesis, and metastasis. *Cancer Res* 2008;68:2850-60.
30. Braconi C, Henry JC, Kogure T, et al. The role of microRNAs in human liver cancers. *Semin Oncol* 2011;38:752-63.
31. Braconi C, Patel T. Non-coding RNAs as therapeutic targets in hepatocellular cancer. *Curr Cancer Drug Targets* 2012;12:1073-80.
32. Braconi C, Patel T. MicroRNA expression profiling: a molecular tool for defining the phenotype of hepatocellular tumors. *Hepatology* 2008;47:1807-9.
33. Braconi C, Valeri N, Gasparini P, et al. Hepatitis C virus proteins modulate microRNA expression and chemosensitivity in malignant hepatocytes. *Clin Cancer Res* 2010;16:957-66.
34. Khan K, Cunningham D, Peckitt C, et al. miR-21 expression and clinical outcome in locally advanced pancreatic cancer: exploratory analysis of the pancreatic cancer Erbitux, radiotherapy and UFT (PERU) trial. *Oncotarget* 2016;7:12672-81.

35. Valeri N, Braconi C, Gasparini P, et al. MicroRNA-135b promotes cancer progression by acting as a downstream effector of oncogenic pathways in colon cancer. *Cancer Cell* 2014;25:469-83.
36. Previdi MC, Carotenuto P, Zito D, et al. Noncoding RNAs as novel biomarkers in pancreatic cancer: what do we know? *Future Oncol* 2017;13:443-453.
37. Julich-Haertel H, Urban SK, Krawczyk M, et al. Cancer-associated circulating large extracellular vesicles in cholangiocarcinoma and hepatocellular carcinoma. *J Hepatol* 2017.
38. Meng F, Henson R, Lang M, et al. Involvement of human micro-RNA in growth and response to chemotherapy in human cholangiocarcinoma cell lines. *Gastroenterology* 2006;130:2113-29.
39. Selaru FM, Olaru AV, Kan T, et al. MicroRNA-21 is overexpressed in human cholangiocarcinoma and regulates programmed cell death 4 and tissue inhibitor of metalloproteinase 3. *Hepatology* 2009;49:1595-601.
40. Wang P, Zou F, Zhang X, et al. microRNA-21 negatively regulates Cdc25A and cell cycle progression in colon cancer cells. *Cancer Res* 2009;69:8157-65.
41. Boj SF, Hwang CI, Baker LA, et al. Organoid models of human and mouse ductal pancreatic cancer. *Cell* 2015;160:324-38.
42. Gao D, Vela I, Sboner A, et al. Organoid cultures derived from patients with advanced prostate cancer. *Cell* 2014;159:176-87.
43. Gjorevski N, Sachs N, Manfrin A, et al. Designer matrices for intestinal stem cell and organoid culture. *Nature* 2016;539:560-564.
44. Moeini A, Sia D, Bardeesy N, et al. Molecular Pathogenesis and Targeted Therapies for Intrahepatic Cholangiocarcinoma. *Clin Cancer Res* 2016;22:291-300.

45. Bhat M, Sonenberg N, Gores GJ. The mTOR pathway in hepatic malignancies. *Hepatology* 2013;58:810-8.
46. Buzzoni R, Pusceddu S, Bajetta E, et al. Activity and safety of RAD001 (everolimus) in patients affected by biliary tract cancer progressing after prior chemotherapy: a phase II ITMO study. *Ann Oncol* 2014;25:1597-603.
47. Lu C, Ward PS, Kapoor GS, et al. IDH mutation impairs histone demethylation and results in a block to cell differentiation. *Nature* 2012;483:474-8.
48. Butler LM, Ferraldeschi R, Armstrong HK, et al. Maximizing the Therapeutic Potential of HSP90 Inhibitors. *Mol Cancer Res* 2015;13:1445-51.
49. Johnson ML, Yu HA, Hart EM, et al. Phase I/II Study of HSP90 Inhibitor AUY922 and Erlotinib for EGFR-Mutant Lung Cancer With Acquired Resistance to Epidermal Growth Factor Receptor Tyrosine Kinase Inhibitors. *J Clin Oncol* 2015;33:1666-73.
50. Sessa C, Shapiro GI, Bhalla KN, et al. First-in-human phase I dose-escalation study of the HSP90 inhibitor AUY922 in patients with advanced solid tumors. *Clin Cancer Res* 2013;19:3671-80.
51. Doi T, Onozawa Y, Fuse N, et al. Phase I dose-escalation study of the HSP90 inhibitor AUY922 in Japanese patients with advanced solid tumors. *Cancer Chemother Pharmacol* 2014;74:629-36.
52. Kim HS, Choo YS, Koo T, et al. Enhancement of antitumor immunity of dendritic cells pulsed with heat-treated tumor lysate in murine pancreatic cancer. *Immunol Lett* 2006;103:142-8.
53. Mbofung RM, McKenzie JA, Malu S, et al. HSP90 inhibition enhances cancer immunotherapy by upregulating interferon response genes. *Nat Commun* 2017;8:451.
54. **Ghidini M, Cascione L, Carotenuto P, et al.** Characterisation of the immune-related transcriptome in resected biliary tract cancers. *Eur J Cancer* 2017;86:158-165.

55. Johnston M, Geoffroy MC, Sobala A, et al. HSP90 protein stabilizes unloaded argonaute complexes and microscopic P-bodies in human cells. *Mol Biol Cell* 2010;21:1462-9.
56. Martinez NJ, Chang HM, Borrajo Jde R, et al. The co-chaperones Fkbp4/5 control Argonaute2 expression and facilitate RISC assembly. *RNA* 2013;19:1583-93.
57. Iki T, Yoshikawa M, Nishikiori M, et al. In vitro assembly of plant RNA-induced silencing complexes facilitated by molecular chaperone HSP90. *Mol Cell* 2010;39:282-91.
58. **Valeri N, Gasparini P**, Braconi C, et al. MicroRNA-21 induces resistance to 5-fluorouracil by down-regulating human DNA MutS homolog 2 (hMSH2). *Proc Natl Acad Sci U S A* 2010;107:21098-103.
59. Claperon A, Mergey M, Nguyen Ho-Boulidoires TH, et al. EGF/EGFR axis contributes to the progression of cholangiocarcinoma through the induction of an epithelial-mesenchymal transition. *J Hepatol* 2014;61:325-32.
60. Scaltriti M, Dawood S, Cortes J. Molecular pathways: targeting hsp90--who benefits and who does not. *Clin Cancer Res* 2012;18:4508-13.
61. Ferraldeschi R, Welti J, Powers MV, et al. Second-Generation HSP90 Inhibitor Onalespib Blocks mRNA Splicing of Androgen Receptor Variant 7 in Prostate Cancer Cells. *Cancer Res* 2016;76:2731-42.
62. Courtin A, Smyth T, Hearn K, et al. Emergence of resistance to tyrosine kinase inhibitors in non-small-cell lung cancer can be delayed by an upfront combination with the HSP90 inhibitor onalespib. *Br J Cancer* 2016;115:1069-1077.
63. Hartl FU, Bracher A, Hayer-Hartl M. Molecular chaperones in protein folding and proteostasis. *Nature* 2011;475:324-32.

Author names in bold designate shared co-first authorship.

**Figure Legend**

**Figure 1. HTS using a library of small molecule compounds in CCA cell lines.** (A) The origin and mutational status of CCA cell lines. (B) HTS was performed using a custom library of 484 compounds. DMSO was used as vehicle control. Cell viability was measured by CellTiter-Blue assay and normalized to that of DMSO. HTS was run at three concentrations in three independent replicates in 6 CCA cell lines. Compounds that significantly inhibited cell proliferation compared with vehicle control ( $p < 0.05$ ) at all three concentrations in each cell line were considered for the graph and number of compounds active per cell line is reported. (C) Data from the HTS relative to the activity of gemcitabine (GEM) in each cell line compared to DMSO. Bars represent mean and SD of three independent replicates.  $p < 0.05$  for all cell lines. (D) Compounds acting on the same target were included in the same class (i.e. HSP90 inhibitors). Compounds that were significantly active in comparison to DMSO ( $p < 0.05$ ) at all three concentrations in each cell line were represented in the radar plot with the radar value representing the number of compounds per class in the selected cell line. Enrichment of selected classes of compounds was identified, such as in the case of HDAC inhibitors in SNU-1079 (all 4 compounds included in the library). In the callout square data without microtubule-targeted compounds and mTOR inhibitors are shown.

**Figure 2. MIR21 expression is associated with sensitivity to HSP90 inhibitors.** (A) Our compound library included 6 and 9 compounds with different degrees of activity on FGFR and HSP90. Changes in cell viability (Log scale) induced by the given compound compared to DMSO are shown. Gemcitabine is reported as positive control. (B) Cells were plated in 384-well plates for 48 hours and AUY922 added at scalar concentrations for 72 hrs. DMSO

was used as control. Cell viability was measured by CellTiter-Blue and  $GI_{50}$  generated through Prism software. (C) MIR21 was assessed in CCA cell lines.  $GI_{50}$  was generated by treating cells with scalar concentrations of AUY922 for 72 hours. Data represent mean of three replicates. (D) Cells were subjected to reverse-transfection and plated in 96 well plates. After 48 hours AUY922 50nM was added. Cell viability was assessed by CellTiter-Blue. Positive control “Cell Death” was used as transfection control. (E) CCLP cells were infected with MIR21 or CTRL TRIPZ viral vector to generate stable clones. miR21 expression was assessed by Taqman assays and normalized to that of RNU48. Bars represent mean and SD of three replicates. (F) Doxycyclin-induced cells were plated in 96 well plates and treated with DMSO or AUY922 (10nM). After 72 hrs doxycycline was removed to deactivate MIR21 expression (indicated by grey area). Cell viability was measured at selected time points by a Celigo S cytometer and plotted against Y axis (DMSO treated cells toward left Y axis, while AUY922-treated cells toward right Y axis). Bars represent SD of 12 replicates. Statistical analysis is reported in Supporting table S4. (G) Representative pictures at different time points are shown.

**Figure 3. DNAJB5 is a target of MIR21.** (A) MIR21 and CTRL TRIPZ viral vector CCLP cells were treated with AUY922 for 72 hours and proteins collected for the HSP array. Dots in the yellow squares represent DNAJB5 protein expression in duplicate. Full details of the antibody plate map are provided below the blots. On the right panel quantification of protein expression, normalized on the averaged positive controls. Bars represent LOG10 of mean and standard deviation of two replicates. Linear fold change of MIR21 vector relative to CTRL vector is 0.89 for HSP60, 0.88 for HSP70, 0.52 for HSP40. (B) Schematic representation of the MIR21 binding site within the 3'UTR of DNAJB5 mRNA (RNAHybrid). (C) MIR21 and CTRL TRIPZ infected CCLP cells were treated with DMSO and AU922 for 72 hours. HSP70

was used a marker of target engagement for AUY922 activity. (D) Cells were plated in 6 well dishes and transfected with a pMirTarget vector containing DNAJB5-3'UTR. Luciferase activity was read after 24 and 48 hours and normalized to renilla activity for each transfected well. Bars represent mean and SD of 3 replicates. (E) Cells were transfected with a plasmid over-expressing DNAJB5 or an empty plasmid pCMV6 for 24 hours, and then treated with AUY922. Cell viability was measured 48 hours later using CellTiter-Blue. Bars represent mean and SD of 6 replicates.

**Figure 4. PDOs were derived from a metastatic patient with chemo-refractory iCCA.**

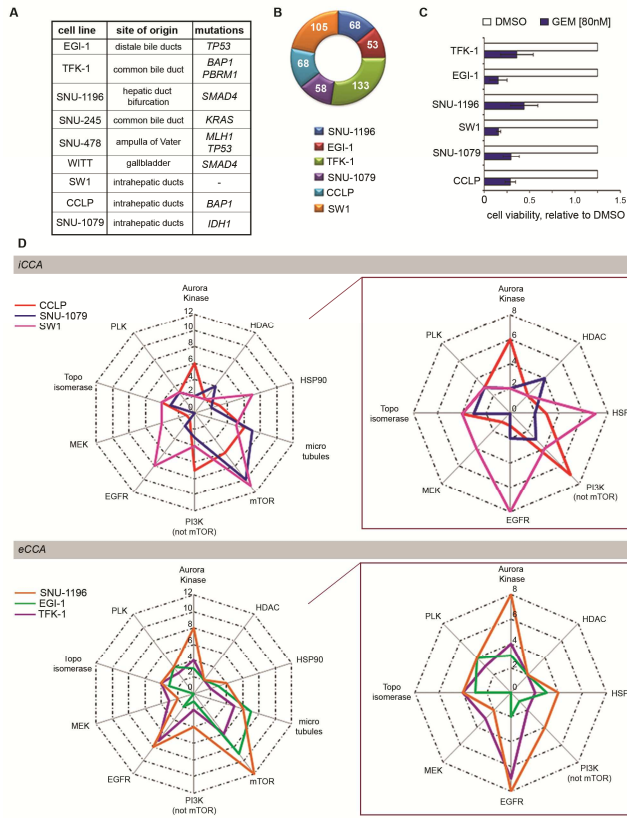
(A) Trend in serum Ca19.9 is represented over time. Biochemical and radiological partial response was observed to chemotherapy with cisplatin and gemcitabine, while progressive disease was recorded after carboplatin-gemcitabine or Folfox chemotherapy. CT (top panel) and PET (bottom panel) images are shown for indicated time points. (B) H&E (left) and IHC for Cytokeratines 7 and 19 (right) of the FFPE research biopsy. Scale bars in  $\mu\text{m}$ .

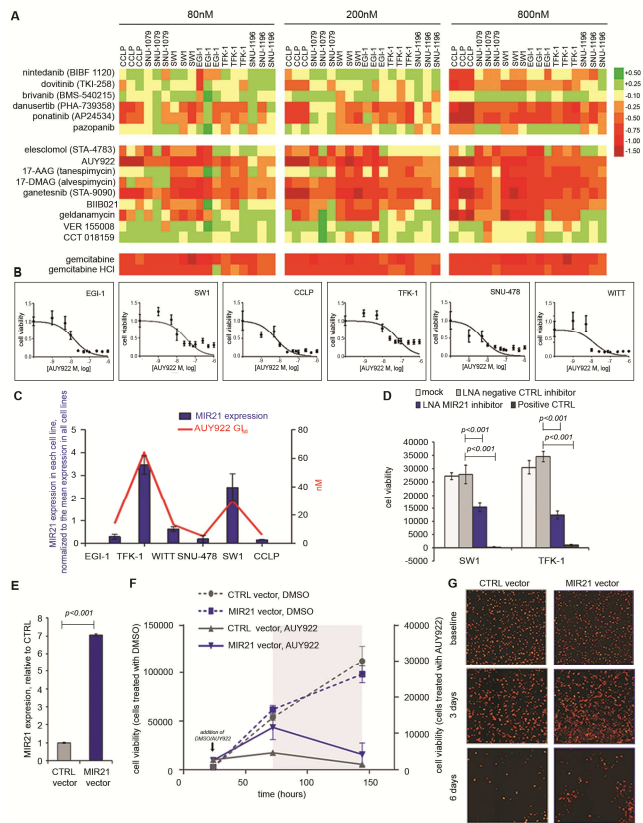
**Figure 5. CCA PDOs sensitivity to HSP90 inhibition with and without MIR21 modulation.**

(A) Phase-contrast images of PDOs derived from one biopsy core of an iCCA. Bars indicate  $100\mu\text{m}$ . (B) One biopsy core was embedded in paraffin, while another core was used to establish PDOs. PDOs were embedded into paraffin and stained for H&E. Bar score in  $\mu\text{m}$ . (C) IHC staining for CK7 and CK19 in PDOs. Bar score in  $\mu\text{m}$ . (D) Total RNA was extracted from the FFPE biopsy and the matching PDOs, and subjected to NanoString analysis. Correlation of gene expression is shown for housekeeping genes (top) and total gene expression (bottom). (E) DNA was extracted from the FFPE biopsy and the matching PDOs and subjected to targeting sequencing. Correlation between Variant Reads Frequency is shown. (F). CCA PDOs were plated in 96-well plates and treated with a number of

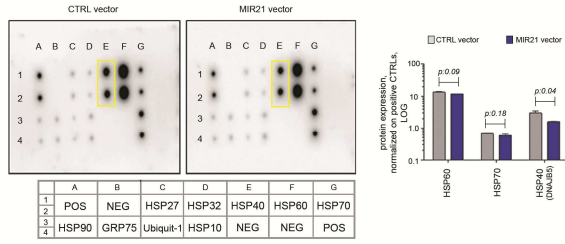
compounds (1 $\mu$ M) in triplicate. Cell viability was tested after 11 days with CellTiter-Blue. Mean of three replicates are shown relative to DMSO with DMSO set at 1. (G) CCA PDOs were treated with scalar concentrations of AUY922 in triplicate. (H) CCA PDOs were infected with a MIR21-inhibitor or control TRIPZ viral vector. RFP+ cells indicate infected cells. Scale bars indicate 100  $\mu$ m. (I) TRIPZ infected CCA PDOs were treated with scalar concentrations of AUY922.

**Figure 6. MIR21 modulation drives sensitivity to AUY922 in CCA PDO-derived animal model.** (A) Schematic representation of *in vivo* studies. Vertical arrows indicate administration of DMSO or AUY922 25 mg/Kg. (B) Tumour growth curves across different groups. Data represent mean and standard error (n: 5 for AUY922 treated, n:4 for DMSO treated). P values are shown in supporting table S5. Grey area represents the period with different diets. (C) HSP70 staining was performed as evidence of target engagement after AUY922 exposure. As expected there was an increase in HSP70 expression after AUY922 treatment but this was not different between the two randomized groups excluding differences in animal dosing. Scale bars: 100  $\mu$ m. (D) Withdrawal of doxycycline diet from mice was associated with a significant inactivation of MIR21 expression and over-expression of DNAJB5. Representative picture of ISH for MIR21 and IHC for DNAJB5 are shown. Scale bars: 100 $\mu$ m. On the right quantification is represented. Bars indicate median with interquartile ranges.





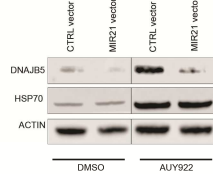
A



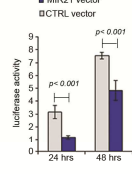
B



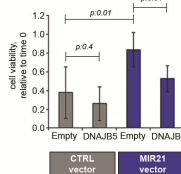
C



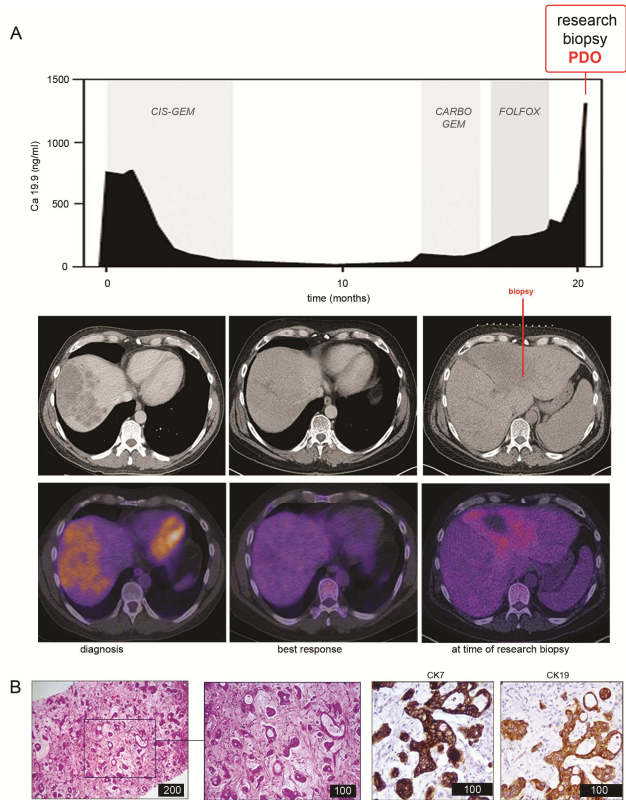
D



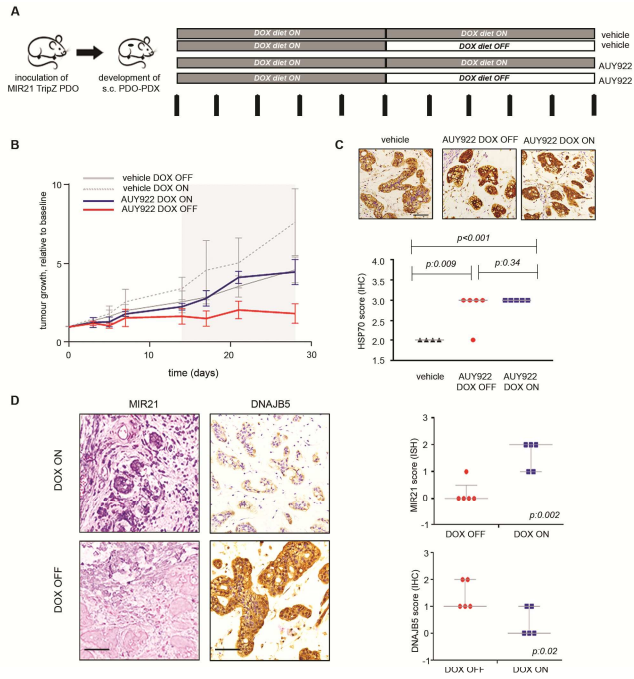
E



ACCEPTED MANUSCRIPT







## SUPPLEMENTARY INFORMATION TO:

**microRNA 21 Promotes Resistance of Cholangiocarcinomas to Heat Shock Protein 90 Inhibitors**

**Short title:** miR-21 as biomarker of HSP90 inhibition

Andrea Lampis<sup>1</sup>, Pietro Carotenuto<sup>1</sup>, Georgios Vlachogiannis<sup>1</sup>, Luciano Cascione<sup>2</sup>, Somaieh Hedayat<sup>1</sup>, Rosemary Burke<sup>1</sup>, Paul Clarke<sup>1</sup>, Else Bosma<sup>1</sup>, Michele Simbolo<sup>3</sup>, Aldo Scarpa<sup>3</sup>, Sijia Yu<sup>1</sup>, Rebecca Cole<sup>1</sup>, Elizabeth Smyth<sup>4</sup>, Javier Fernández Mateos<sup>1</sup>, Ruwaida Begum<sup>4</sup>, Blanka Hezelova<sup>4</sup>, Zakaria Eltahir<sup>4</sup>, Andrew Wotherspoon<sup>4</sup>, Nicos Fotiadis<sup>4</sup>, Maria Antonietta Bali<sup>4</sup>, Chirag Nepal<sup>5</sup>, Khurum Khan<sup>5</sup>, Mark Stubbs<sup>1</sup>, Jens C Hahne<sup>1</sup>, Pierluigi Gasparini<sup>6</sup>, Vincenza Guzzardo<sup>7</sup>, Carlo M Croce<sup>6</sup>, Suzanne Eccles<sup>1</sup>, Matteo Fassan<sup>3,7</sup>, David Cunningham<sup>4</sup>, Jesper B Andersen<sup>5</sup>, Paul Workman<sup>1</sup>, Nicola Valeri<sup>1,4</sup>, Chiara Braconi<sup>1,4</sup>

**Supplementary methods**

**Cell lines.** Intrahepatic (SW1, SNU-1079, CCLP), and extrahepatic (SNU-1196, TFK-1, EGI-1, SNU-245) CCA cell lines, along with gallbladder (WITT) and Ampulla of Vater (SNU-478) cancer cell lines, were purchased from the Leibniz Institute DSMZ-German Collection of Microorganisms and Cell Culture (Braunschweig, Germany), the Korean Cell Line Bank (Seoul, Korea) or were kindly provided by Prof. Stuart Forbes (University of Edinburgh). Cells were cultured in Dulbecco's modified Eagle medium with 10 % foetal bovine serum. MIR21KO RKO colon carcinoma cells were purchased from Horizon Discovery (Cambridge, UK), while MIR21KO DLD-1 colon carcinoma cells were a kind gift from Jian Yu (University of Pittsburgh Cancer Institute) to Carlo Croce (Ohio State University). Cells were tested negative for Mycoplasma and authenticated through Short Tandem Repeat (STR) analysis.

**Next generation sequencing of multiplex PCR amplicons.** Two multigene panels were used: the 50-gene Ion AmpliSeq Cancer Hotspot panel v2 (Life Technologies, Paisley, UK) and an AmpliSeq custom panel targeting six genes not included in the commercial panel, as previously described<sup>1</sup>. The first explores selected regions of 50 cancer- genes: ABL1, AKT1, ALK, APC, ATM, BRAF, CDH1, CDKN2A, CSF1R, CTNNB1, EGFR, ERBB2, ERBB4, EZH2, FBXW7, FGFR1, FGFR2, FGFR3, FLT3, GNA11, GNAS, GNAQ, HNF1A, HRAS, IDH1, IDH2, JAK2, JAK3, KDR/VEGFR2, KIT, KRAS, MET, MLH1, MPL, NOTCH1, NPM1, NRAS, PDGFRA, PIK3CA, PTEN, PTPN11, RB1, RET, SMAD4, SMARCB1, SMO, SRC, STK11, TP53, VHL. The custom panel targets additional 6 genes: ARID1A, BAP1, PBRM1, PIK3C2A, PIK3C2G, TGFBR2. Twenty 20 ng of DNA was used for each multiplex PCR amplification. Emulsion PCR was performed with the OneTouch2 system (Life Technologies, Paisley, UK). The quality of the libraries was evaluated by on-chip electrophoresis in an Agilent Technologies' 2100 Bioanalyzer (Santa Clara, USA). Sequencing was run on an Ion Torrent Personal Genome Machine (Life Technologies, Paisley, UK) loaded with 316 (50-gene panel) or 318 chips (6-gene panel). Data analysis, including alignment to the hg19 human reference genome and variant calling, was done using the Torrent Suite Software v.3.6 (Life Technologies, Paisley, UK). Filtered variants were annotated using the SnpEff software v.3.1<sup>2</sup>. Alignments were visually verified with the Integrative Genomics Viewer v.2.2<sup>3,4</sup>.

**Bioinformatics.** For all statistical analyses the R language environment was used (v. 3.0.1; www.r-project.org). Hierarchical clustering was performed on cell viability data using the Pearson correlation as metric and complete linkage as method. We determined significant associations ( $p < 0.05$ ) between a selected mutation and drug sensitivity by Chi-square test with the Yates correction factor.

**Real time PCR.** RNA was extracted using Trizol (Invitrogen, Carlsbad, USA). Reverse transcription was performed with Taqman microRNA reverse transcription kit (Life Technologies, Paisley, UK ), and miRNA expression assessed by qPCR with Taqman assay and normalized to that of RNU48 (Life Technologies, Paisley, UK)

**Transfection.** Cells were reversed transfected in 96-well plates using HiPerFect Transfection Reagent Qiagen, Hilden, Germany). For transient inhibition of miR-21 a locked nucleic acid (LNA<sup>TM</sup>) miR-21 inhibitor or the Negative Control A LNA were used (Exiqon, Vedbaek, Denmark). In rescue experiments cells were transfected with DNAJB5-pCMV6 or Empty-pCMV6 (Origene, Rockville, MD, USA).

**Cell viability.** Cell viability was measured by CellTiter-Blue® Assay (Promega, Madison, WI, USA) and the GI<sub>50</sub> derived using Prism Software (Graphpad, La Jolla, USA). For RFP+ cells cell viability was assessed by Incucyte Zoom live cell imaging (Essen Bioscience, Hertfordshire, UK) or by Celigo S (Nexcelom, Manchester, UK).

**Live cell imaging.** Cells were plated in 96-well plates and monitored with IncuCyte Zoom (Essen Bioscience, Hertfordshire, UK). Phase-contrast images and RFP+ images were taken every 4 hours.

**Tetracycline-activated (Tet-on) inducible stable clones.** The precursor miR-21 sequence was cloned into a TRIPZ lentivector (Dharmacon, Little Chalfont, UK) using PCR amplification of target region and digestion with Cla I and Mlu I restriction enzymes (New England Biolabs, Ipswich, Massachusetts, USA). Packaging of viral particles and target cell lines

infections were performed using HEK293T. Overexpression of miR-21 was confirmed by Taqman assay. Plasmid with anti-miR-21 sequence was produced by amplification and cloning of anti-miR-21 sequence, with standard cloning procedures, from miRZip<sup>TM</sup>-miR-21 plasmid (System Bioscience, Palo Alto, CA, USA) in order to generate an equivalent inducible system for silencing miR-21 expression. Cell growth optimization for plating density has been performed for cells with miR-21 manipulation to take into consideration the effect of miR-21 on cell growth.

**Human heat shock protein antibody array.** Cells were solubilized in 1X lysis buffer containing a protease inhibitor cocktail. Membrane antibody arrays (RayBiotech, Norcross, USA) were blocked with 1 mL of blocking buffer for 30 min. 500 µg of extracted proteins were diluted in 1 mL of blocking buffer and dispersed on top of membrane antibody arrays overnight at 4 °C. Detection was performed as per the manufacturer's instructions and the signal measured using Licor system (Licor, Lincoln, NE, USA).

**Western blot.** Immunoblotting was performed as previously described<sup>5</sup>. Incubation with primary antibodies for DNAJB5 (ab101514, Rabbit; Abcam, 1:1000 dilution), HSP70 (ab182844, Rabbit, Abcam; 1:5000 dilution), Beta-Actin (Anti-Actin, Clone C4, Mouse, MP Biomedicals; 1:10000 dilution) was performed overnight at 4°C. Secondary HRP-conjugated polyclonal Goat Anti-Rabbit or Goat Anti-Mouse antibodies (Cell Signaling, Danvers, MA, USA; 1:10000) were used. Prime ECL (Amersham, GE healthcare) was used to develop signal as manufacturer's instructions with Licor imaging system.

**Luciferase assays.** Cells were transfected with 1 µg DNAJB5-pMirTarget or pMirTarget CTRL (Origene, Rockville, USA) with HiPerFect Transfection Reagent (Qiagen, Hilden,

Germany) and the luciferase activity measured after 48 h using the Dual Glo Assay system (Promega, Madison, WI, USA) according to the manufacturer's protocol in a multiwell plate luminometer (Perkin-Elmer, Seer Green, Beaconsfield, UK). Luciferase activity was normalized to that of renilla activity for each transfected well.

**Immunohistochemistry:** Immunohistochemical stains were automatically performed in 3-4  $\mu\text{m}$  sections using the Bond Polymer Refine Detection kit (Leica Biosystems, Newcastle upon Tyne, UK) in the BOND-MAX system (Leica Biosystems), according to the manufacturer's specifications. Appropriate positive and negative controls were run concurrently. The following antibodies were used: DAKO mouse monoclonal CK7 (Agilent, Santa Clara, CA, USA), DAKO mouse monoclonal CK19 (Agilent, Santa Clara, CA, USA), rabbit polyclonal DNAJB5 (Sigma-Aldrich, Haverhill, UK) and rabbit polyclonal HSP70 (Abcam, Cambridge, UK). DNAJB5 was classified according to a 4-tiered scoring system based on the intensity of protein expression as follows: 0: indicates no stain or stain in less than 10% of tumour cells; 1+: faint/weak cytoplasm/nuclear stain in 10% or more of cells; 2+: moderate cytoplasm/nuclear stain in 10% or more of tumour cells; and 3+: strong cytoplasm/nuclear stain in 10% or more of tumour cells.

**In Situ RNA hybridization.** A locked nucleic acid (LNA) probe with complementarity to a 21-bp section of miR-21 was labelled with 5'-digoxigenin and synthesized by Exiqon. Tissue sections were digested with ISH protease 1 (Ventana Medical Systems) and *in situ* hybridization performed as described<sup>6</sup>. Negative controls included omission of the probe and the use of a scrambled LNA probe. Each sample was classified according to a 4-tiered scoring system based on the intensity of miR-21 expression as follows: 0: indicates no stain or stain in less than 10% of tumour cells; 1+: faint/weak cytoplasm/nuclear stain in 10% or

more of cells; 2+: moderate cytoplasm/nuclear stain in 10% or more of tumour cells; and 3+: strong cytoplasm/nuclear stain in 10% or more of tumour cells. In all the considered tissue samples, fibroblasts featured miR-21 expression and were assumed as positive internal control (not considered in ISH score).

### **Supporting Table legend**

***Supporting Table 1.*** List of drugs included in the library used for the HTS.

***Supporting Table 2.*** Comparison between mutations found in human CCA tissues and human CCA cell lines using the same NGS gene-panel. Mutations that were found to be present in >10% of human tissue are shown in the left column<sup>1</sup>; mutations that are represented in our cell lines are depicted with an “x”.

***Supporting Table 3.*** List of drugs that were statistically significantly ( $p < 0.05$ ) active at all the 3 concentration in each cell line. Compounds that are commonly represented across all the iCCA or the eCCA cell lines are depicted in yellow and light blue respectively.

***Supporting Table S4.*** Statistical analysis of experiments in Fig 2E. P value indicates unpaired two-tailed test. Fold changes (FC) in cell viability are reported for day 3 that represents the timepoint at which the assessment of response was performed following miR-21 over-expression.

***Supporting Table 5.*** Statistical analysis of animal experiments. P value indicates unpaired two-tailed test.

**Supporting video legends**

**Video 1.** miR-21KO DLD1 cells were stably infected with an inducible viral vector over-expressing miR-21 or CTRL. Cells were exposed to doxycycline (1 $\mu$ g/ml) to activate miR-21/CTRL and RFP expression that were under the same promoter. RFP+ (red) cells represented activated infected cells. Activated cells were plated in 96-well plates and AUY-922 added 22 hrs later. Cell viability and RFP confluency were monitored and measured at interval periods through the Incucyte Zoom. Data represent mean and STDEV of 12 replicates.

**Video 2.** miR-21KO DLD1 cells were co-cultured with Tet-on miR-21KO miR-21 vector DLD-1 cells. Cells were activated, plated in 96-well plate, exposed to doxycycline, and treated with AUY-922. RFP+ cells represented cells that over-expressed miR-21, while RFP- (bright-field) cells represented miR-21KO cells.

**Supporting figure legends**

**Supporting Figure 1.** (A&B) Hierarchical clustering based on the sensitivity (green) or resistance (red) of cells to small molecule inhibitors. Cells were considered sensitive if a compound reduced cell viability >20%, compared to DMSO, across 3 replicates. A Chi<sup>2</sup> test was used to identify significant correlations between mutations and drug sensitivity. Mutated cells clustered together, independently of tumour origin [eCCA (light blue) vs iCCA (black)]. Of note, a concentration-response effect was observed [80nM (yellow), 200nM (orange), 800nM (red)].

**Supporting Figure 2.** (A&B) Data from the 200 nM compound screening in RKO cells are shown as a colour map or a bar graph. Bars represent mean and standard deviation of three replicates. (C&D) Cells were plated in 96-well plates for 24 hours and AUY922 added at scalar concentrations for 72 hrs. DMSO was used as control. Cell viability was measured by CellTiter-Blue and GI<sub>50</sub> generated through Prism software. Bars represent mean and SD of 6 replicates. (E) Cell were treated with the same concentration of AUY922 (10nM) for 72 hours and cell viability assessed by CellTiter-Blue. Bars represent mean and SD of 6 replicates. (F) miR21 expression was assessed by Taqman assays and normalized to that of RNU48. Bars represent mean and SD of three replicates. Baseline miR-21 expression is higher in RKO compared to DLD-1 WT cells.

**Supporting Figure 3.** (A) miR-21KO DLD-1 cells were stably infected with a Tet-on TRIPZ vector enabling over-expression of miR-21 and RFP, or a control (CTRL) empty vector expressing RFP. Cells were exposed to doxycycline to induce miR-21/CTRL and RFP expression that were under the same promoter. RFP+ (red) cells represented induced infected

cells. Induced cells were plated in 96-well plates and AUY922 added 22 hrs later. Cell viability and RFP confluency were monitored and measured at intervals by the Incucyte Zoom. Data represent mean and STDEV of 12 replicates. Difference between the two curves was statistically significant ( $p < 0.05$ ). Representative images are shown for selected time points. (B) miR-21KO DLD1 cells were co-cultured with Tet-on miR-21KO miR-21 vector DLD-1 cells. Cells were induced, plated in 96-well plate, exposed to doxycycline, and treated with AUY922 (10nM). RFP+ cells represented cells that over-expressed miR-21, while RFP- (bright-field) cells represented miR-21KO cells. Phase contrast and RFP confluency were monitored and measured at intervals by the Incucyte Zoom. Cell proliferation was reduced in RFP- cells, while RFP+ cells were able to expand and proliferate. Images are shown for selected time points.

**Supporting Figure 4.** EGI-1 cells were infected with miR-21 or CTRL TRIPZ viral vector to generate inducible stable clones. (A) miR21 expression was assessed by Taqman assays and normalized to that of RNU48. Bars represent mean and SD of three replicates. (B) doxycyclin-activated cells were plated in 96 well plates and treated with sub-lethal concentrations of AUY-922 (5nM). After 72 hrs doxycycline was removed to deactivate miR-21 expression. Cell viability was measured at selected time points by Celigo S. Bars represent mean and SD of 12 replicates.

**Supporting Figure 5.** CRC PDOs were plated in 96-well plates and treated with AUY922 in triplicates at 20nM (A) or at scalar concentrations (B). (C) CRC PDOs were infected with a miR-21-over-expressing or control TRIPZ viral vector. (D) TRIPZ infected CRC PDOs were treated with scalar concentrations of AUY922. miR-21 expressing cells were more resistant to AUY922.

**Supplementary references**

1. Simbolo M, Fassan M, Ruzzenente A, et al. Multigene mutational profiling of cholangiocarcinomas identifies actionable molecular subgroups. *Oncotarget* 2014;5:2839-52.
2. Cingolani P, Platts A, Wang le L, et al. A program for annotating and predicting the effects of single nucleotide polymorphisms, SnpEff: SNPs in the genome of *Drosophila melanogaster* strain w1118; iso-2; iso-3. *Fly (Austin)* 2012;6:80-92.
3. Robinson JT, Thorvaldsdottir H, Winckler W, et al. Integrative genomics viewer. *Nat Biotechnol* 2011;29:24-6.
4. Thorvaldsdottir H, Robinson JT, Mesirov JP. Integrative Genomics Viewer (IGV): high-performance genomics data visualization and exploration. *Brief Bioinform* 2013;14:178-92.
5. Carotenuto P, Fassan M, Pandolfo R, et al. Wnt signalling modulates transcribed-ultraconserved regions in hepatobiliary cancers. *Gut* 2017;66:1268-1277.
6. Braconi C, Valeri N, Kogure T, et al. Expression and functional role of a transcribed noncoding RNA with an ultraconserved element in hepatocellular carcinoma. *Proc Natl Acad Sci U S A* 2011;108:786-91.

Supporting Table S1. List of drugs included in the library used for the HTS.

ABT-263 (Navitoclax)	PIK-90	Fingolimod (FTY720) HCl	Desmethyl Erlotinib (CP-473420)
ABT-737	Anastrozole	GDC-0152	Torin 1
Linifanib (ABT-869)	Aprepitant	Birinapant	PF-562271
Veliparib (ABT-888)	Bicalutamide	Stattic	S-Ruxolitinib (INCB018424)
Axitinib	Fulvestrant	EP25676	BAY 11-7082
Saracatinib (AZD0530)	Raltitrexed	IWR-1-endo	CHIR-99021 (CT99021) HCl
Selumetinib (AZD6244)	Thalidomide	UNC1215	Pazopanib
BEZ235 (NVP-BEZ235)	CUDC-101	SCH772984	Daunorubicin HCl
Nintedanib (BIBF 1120)	Exemestane	NLG919	BMS-833923
Afatinib (BIBW2992)	Irinotecan	LDN-57444	TCID
Bortezomib (PS-341)	Cladribine	Azacitidine	LGK-974
Bosutinib (SKI-606)	Decitabine	Teniposide	AVL-292
Cediranib (AZD2171)	Dimesna	Simvastatin	SKI II
Dovitinib (TKI-258)	PIK-75	Ranolazine	AGI-5198
PD184352 (CI-1040)	Tivozanib (AV-951)	Lomustine	RepSox
Dasatinib	Doxorubicin (Adriamycin)	D-glutamine	Ferrosstatin-1 (Fer-1)
Ridaforolimus (Deforolimus)	Fluorouracil (5-Fluoracil)	Hydroxyurea	KPT-330
Erlotinib HCl (OSI-744)	Methotrexate	Flutamide	SGC-CBP30
Gefitinib (ZD1839)	Imiquimod	Fluvastatin Sodium	MM-102
Imatinib Mesylate (STI571)	Bendamustine HCl	Tamoxifen Citrate	478C
Lapatinib (GW-572016) Ditosylate	Nelarabine	Procabazine hydrochloride (Matulane)	IWP-L6
Lenalidomide (CC-5013)	Bleomycin Sulfate	Sodium butyrate	GSK2606414
Panobinostat (LBH589)	Carboplatin	Maraviroc	WZ4003
Motesanib Diphosphate (AMG-706)	Cyclophosphamide	PF-573228	AZ191
Nilotinib (AMN-107)	Clofarabine	Cyclophosphamide Monohydrate	UNC2250
PD0325901	YM201636	Bexarotene	SMI-4a
PI-103	OSI-930	Vinpocetine (Cavinton)	GW0742
Rapamycin (Sirolimus)	Dacarbazine	Lapatinib	Empagliflozin (BI 10773)
Sorafenib Tosylate	Epirubicin HCl	Neratinib (HKI-272)	GSK3787
STF-62247	Oxaliplatin	LDE225 (NVP-LDE225)	Plerixafor (AMD3100)
Sunitinib Malate	Etoposide	AG-14361	BMS-345541
Tandutinib (MLN518)	KU-0063794	MLN2238	Macitentan
Temsirolimus (CCI-779)	Raloxifene HCl	MLN9708	1,4-PB-ITU dihydrobromide
Trichostatin A (TSA)	Idarubicin HCl	SB743921	4-Phenylbutyrate
Vandetanib (ZD6474)	Fludarabine Phosphate	GSK461364	Anagrelide
Vorinostat (SAHA)	Topotecan HCl	SGI-1776 free base	Apicidin
VX-680 (Tozasertib	2-Methoxyestradiol (2-MeOE2)	BMS-794833	AR-A 014418
Y-27632 2HCl	Letrozole	OSI-420	AZ 23
Elesclomol (STA-4783)	Leucovorin Calcium	R788 (Fostamatinib) Disodium	Banaxtrone dihydrochloride
Entinostat (MS-275)	Temozolomide	Formestane	Bay 11-7085
Enzastaurin (LY317615)	Vincristine	DAPT (GSI-IX)	BAY 61-3606
AC480 (BMS-599626)	Amuvatinib (MP-470)	Irinotecan HCl Trihydrate	BD 1047
Obatoclox Mesylate (GX15-070)	Vinblastine	CYT387	BI 78D3
Olaparib (AZD2281)	JNJ-7706621	SB590885	BIX 01294
Nutlin-3	Enzalutamide (MDV3100)	TAME	BML-266
Masitinib (AB1010)	Celecoxib	CAL-101 (Idelalisib)	BML-277
GDC-0941	PD173074	LY2157299	C 646
SB431542	WYE-354	Telatinib	CAY10581
Crizotinib (PF-02341066)	Vemurafenib (PLX4032)	Volasertib (BI 6727)	CAY10626
AUY922 (NVP-AUY922)	IC-87114	Palomid 529 (P529)	CCT 018159
PHA-665752	BX-795	Degrasyn (WP1130)	CD 437
ZSTK474	Altretamine	AR-42	CDIBA
SB216763	Carmofur	CP-466722	CGP 3466B
SB203580	Epothilone A	BKM120 (NVP-BKM120)	CGS 9343B
MK-2206 2HCl	Floxuridine	CX-4945 (Silmitecaterib)	Combretastatin A4
PD153035 HCl	FT-207 (NSC 148958)	(-)-Epigallocatechin Gallate	cPEPCK inhibitor
SU11274	Ifofosamide	Cyclosporin A	DAG Kinase Inhibitor
Vismodegib (GDC-0449)	Megestrol Acetate	Gossypol	DFMO
Brivanib (BMS-540215)	Mercaptopurine (6-MP)	Phloretin	EBPC
Belinostat (PXD101)	Pamidronate Disodium	Salinomycin	Elacridar
Iniparib (BSI-201)	Streptozotocin (STZ)	Quercetin	Farnesyl Thiosalicylic Acid
PCI-24781 (Abexinostat)	Dexamethasone (DHAP)	Coenzyme Q10(CoQ10)	Fenretinide
OSI-906 (Linsitinib)	Rigosertib (ON-01910)	Chrysophanic Acid	FR 180204
KU-55933 (ATM Kinase Inhibitor)	Epothilone B (EPO906)	Imatinib (STI571)	GANT 61
GSK1904529A	Bafetinib (INNO-406)	Itraconazole	GSK 264220A
PF-04217903	Dorzolamide HCl	Mitoxantrone HCl	GSK 269962
Quisinosat (JNJ-26481585)	Ruxolitinib (INCB018424)	Mycophenolic acid	GSK 3787
BTZ043 Racemate	Isotretinoin	Rosiglitazone	GSK 650394
Rucaparib (AG-014699)	Pelitinib (EKB-569)	Medroxyprogesterone acetate	GSK837149A
Vatalanib (PTK787) 2HCl	AS-605240	Pioglitazone	GW 9508
GDC-0879	Zileuton	Mifepristone	HLI 373
LY294002	Ispinesib (SB-715992)	Lonidamine	Hypoxia Inducible Factor-1a Inhibitor
Danusertib (PHA-739358)	Tipifarnib	TAK-733	ICI 182
TAE684 (NVP-TAE684)	Zibotentan (ZD4054)	LDN193189	ITX 3
BI 2536	AZD6482	LY2603618	Ivactin
SGX-523	Doxercalciferol	GW3965 HCl	JAK3 Inhibitor VI
GSK690693	SB525334	DCC-2036 (Rebastinib)	JK 184
JNJ-38877605	AEE788 (NVP-AEE788)	NU7441 (KU-57788)	JNK Inhibitor V
Palbociclib (PD-0332991) HCl	PHA-793887	GSK2126458 (GSK458)	JZL 184
Triciribine	PIK-93	MK-0752	Lck Inhibitor
XL147	Ponatinib (AP24534)	PF-3845	LG 100268
Everolimus (RAD001)	Fludarabine	Trametinib (GSK1120212)	L-NNA
TW-37	LY2228820	Flavopiridol HCl	Lomeguatrib
Mocetinostat (MGCD0103)	Mycophenolate Mofetil	Ibrutinib (PCI-32765)	LY 320135
Abiraterone (CB-7598)	Pracinostat (SB939)	NVP-BSK805 2HCl	LY 333531
SRT1720	Tosedostat (CHR2797)	XL335	Marimastat
YM155 (Sepantronium Bromide)	SAR245409 (XL765)	GDC-0980 (RG7422)	MG 149
Alisertib (MLN8237)	AT7519	A-769662	ML 141
AT9283	MK-1775	CH5132799	MRT-10
Pemetrexed	Quizartinib (AC220)	KX2-391	Necrostatin-1
Andarine	Vinorelbine	LY2109761	NF7B Activation Inhibitor III
17-AAG (Tanespimycin)	AZD7762	YO-01027	NSC 23766
17-DMAG (Alvespimycin) HCl	R406 (free base)	Geldanamycin	NSC 663284
SNS-032 (BMS-387032)	DMXAA (Vadimezan)	AMG-900	NU6027
Cyclopamine	EX 527 (Selisistat)	PF-03814735	Oxamflatin

Barasertib (AZD1152-HQPA)	Febuxostat	PH-797804	PB 28 dihydrochloride
Docetaxel	Dapagliflozin	Dacomitinib (PF299804)	PD 166285
Gemcitabine HCl (Gemzar)	AZD8055	Crenolanib (CP-868596)	Pentostatin
Paclitaxel	BMS-777607	AZ 3146	PF 477736
Roscovitine (Seliciclib)	Pomalidomide	TG101348 (SAR302503)	PF-4708671
SNS-314 Mesylate	KU-60019	PAC-1	PIM-1 Inhibitor 2
Capecitabine	BIRB 796 (Doramapimod)	AZ 628	Pyroxamide
Ganetespib (STA-9090)	Tie2 kinase inhibitor	AT-406	QNZ
Lenvatinib (E7080)	Ubenimex (Bestatin)	Canagliflozin	S-(-)-Niguldipine hydrochloride
ABT-751 (E7010)	Prednisone	3-Methyladenine	SA4503
Cisplatin	Triamcinolone Acetonide	Dalcecrapib (JTT-705)	SANT-1
Sodium valproate	Cytarabine	Nocodazole	SANT-2
TGX-221	Tretinoin	GW4064	SB 265610
CYC116	Ezetimibe	Tofacitinib (CP-690550)	SCH 79797
JNJ-26854165 (Serdemetan)	Estrone	Sotrastaurin	SecinH3
WZ4002	Aminoglutethimide	APO866 (FK866)	SID 7969543
MK-2866 (GTx-024)	Disulfiram	Sirtinol	SJ 172550
BIIB021	Meprednisone	CEP-33779	SK1-1
Plinabulin (NPI-2358)	Busulfan	INK 128 (MLN0128)	SKF 91488
Regorafenib (BAY 73-4506)	Hydrocortisone	BYL719	SKI II
XAV-939	Estradiol	Torin 2	SMER 3
ENMD-2076	Gemcitabine	RG108	SR 33805
BIBR 1532	Azathioprine	TPCA-1	Src 11
Anagrelide HCl	Mesna	U 73122	STAT5 Inhibitor
Triptolide (PG490)	Toremifene Citrate	UNC 0224	TCS PIM-1 4a
QNZ (EVP4593)	Dexamethasone acetate	VER 155008	TTP 22

Supporting Table S2. Comparison between mutations found in &gt;10% of human CCA tissues (as pe

MUTATED GENE	% in ICCA	% in eCCA	PRESENT IN CELL LINES
ARID1	11.4	12.3	
BAP1	14.3		X
IDH1	15.7		X
KRAS	15.7	47.4	X
PBRM1	14.3		X
SMAD4		10.5	X
TP53		17.5	X

r Simbolo et al) and our human CCA cell lines using the same NGS gene-panel.

ACCEPTED MANUSCRIPT



**Supporting Table S4. Statistical analysis of experiments in Fig 2 E.** P value indicates unpaired two-tailed ttest. Fold changes (FC) in cell viability are reported for day 3 that represents the timepoint at which the assessment of response was performed following miR-21 over-expression.

	baseline (24 hours)	DAY 3 (72 hours)	DAY 6 (144 hours)
CTRL, AUY922 vs miR-21, AUY922 (p value)	0.31	3.30E-10 <i>FC (LOG) miR21/CTRL: 0.40</i>	0.001
CTRL, DMSO vs miR-21, DMSO (p value)	0.32	1.70E-05 <i>FC (LOG) miR21/CTRL: 0.06</i>	0.01
CTRL, DMSO vs CTRL, AUY922 (p value)	0.3	2.80E-32 <i>FC (LOG)AUY922/DMSO: -1.06</i>	3.00E-23
miR-21, DMSO vs miR-21, AUY922 (p value)	0.3	3.90E-25 <i>FC (LOG) AUY922/DMSO: -0.72</i>	9.40E-23

**Supporting Table S5. Statistical analysis of animal experiments.** P value indicates unpaired two-tailed ttest.

Vehicle (averaged) indicates the average of DOX-ON and DOX-OFF mice.

	baseline	DAY 5	DAY 7	DAY 14	DAY 17	DAY 21	DAY 28
AUY922 DOX-OFF vs AUY922 DOX ON	0.29	0.50	0.67	0.29	0.10	0.02	0.03
vehicle DOX-OFF vs vehicle DOX ON	0.21	0.80	0.55	0.43	0.40	0.42	0.23
vehicle (averaged) vs AUY922 DOX-ON	0.14	0.37	0.40	0.28	0.48	0.89	0.39
vehicle (averaged) vs AUY922 DOX-OFF	0.10	0.15	0.31	0.07	0.12	0.09	0.02



